An Acad Bras Cienc (2021) 93(Suppl. 4): e20210081 DOI 10.1590/0001-3765202120210081
Anais da Academia Brasileira de Ciências | *Annals of the Brazilian Academy of Sciences*
Printed ISSN 0001-3765 I Online ISSN 1678-2690
www.scielo.br/aabc | www.fb.com/aabcjournal

GEOSCIENCES

Bouguer anomaly inversion and hydrocode modeling of the central uplift of the Araguainha impact structure

MARCELLE R. MIYAZAKI, EMILSON P. LEITE, MARCOS A.R. VASCONCELOS, KAI WÜNNEMANN & ALVARO P. CRÓSTA

Abstract: Araguainha is a mid-sized complex impact structure formed in sedimentary and underlying basement rocks of the Paraná Basin, Brazil. The structure has strongly deformed sedimentary strata surrounding a granitic core. The central uplift is a region of high geological complexity, comprising different types of sedimentary, igneous (granite) and metamorphic lithologies, plus breccias and impact melt sheets. New ground gravity data was collected to produce a Bouguer anomaly map and to perform a 3-D inversion in order to obtain a 3-D density model of the central uplift. This 3-D density model is consistent with iSALE numerical modeling results, which shows that the rocks in the innermost portion became brecciated and/or melted after undergoing pressure/temperature peaks. The positive anomaly of Furnas and Ponta Grossa formations associated with the numerical model shows that the central uplift is ~16 km wide. Thus, the granite's uplift caused the uplift of the entire stratigraphic package, from its Devonian-aged units to the Permian ones, forming a bull's eye pattern around the granitic core. The results also indicate that Araguainha was formed by a 3 km diameter impactor, and the rocks of the granitic basement rocks were uplifted by ~2 km.

Key words: 3D density model, Araguainha impact structure, gravimetry, impact crater.

INTRODUCTION

Impact structures are found on all solid planetary bodies, and play an important role in the formation and evolution of planetary landscapes. Understanding the processes through which impact structures are formed helps to reveal how the planet evolved over geological time, particularly its shallower layers.

There are different types of diagnostic features used to prove the impact origin of a given structure. Some features are exclusively formed under high pressure conditions, such as shatter cones, planar fractures, tectosilicates with planar features, high-density minerals ranging from quartz to graphite, and transformation of minerals into amorphous phases, such as glass/lechatelierite (Melosh 1989, French 1998, Crósta et al. 2019). However, as the Earth is one of the most geologically active planetary bodies among all terrestrial objects in the solar system, impact structures are often poorly preserved and difficult to identify due to processes such as erosion, sedimentation, and tectonic movements that obliterate the geological record of impact events (Reimold et al. 2018, Crósta et al. 2019).

Most of the known impact structures on Earth are partially eroded and/or covered by post-impact sedimentary rocks. This is usually the case of the seven impact structures found in Brazil, formed in the Phanerozoic Paraná Basin (Araguainha, Vargeão, Vista Alegre and Cerro do

Jarau impact structures) and Parnaíba Basin (Serra da Cangalha, Riachão, and Santa Marta impact structures), the records of which are generally restricted to morphology and some sort of deformation, and more rarely to molten rocks (Crósta et al. 1981, Engelhardt et al. 1992, Silva et al. 2016). Geophysical investigations often provide signatures that may have resulted from shock-induced physical changes, indicating features that are missing from the geological record (Ernstson 1984, Ivanov & Stöffler 2005).

Gravimetry is a geophysical method that uses information from the gravitational field in a given area on a planet's surface, seeking anomalies related to variations in the density and extent of lithological units in subsurface. Specifically, in the case of impact structures, these anomalies might have been caused by changes experienced by the local country rocks, and in the degree of fractures and/or uplift of underlying layers. Although gravity anomalies cannot prove a structure's origin, they can be used to estimate the original size of heavily-eroded structures (Ernstson et al. 1978).

The most common geophysical characteristic associated with terrestrial impact structures is a negative Bouguer anomaly commonly related to the low-density material (breccias and brecciated rocks) produced by lithological and physical changes related to the cratering process (Pilkington & Grieve 1992, Grieve & Pilkington 1996). However, some impact structures may exhibit local positive Bouguer anomalies in their center, surrounded by a bowl-shaped gravity low. Depending on the level of erosion, these gravity lows are generally circular in shape, and extend to, or slightly beyond, the rim of the structure (Pilkington & Grieve 1992).

Previous studies have addressed the gravity signature of the Araguainha impact structure (Marangoni et al. 2007, Vasconcelos 2007), but the results were not as expected for structures with similar size. Usually, large impact structures exhibit a proportional positive anomaly, something that does not happen in Araguainha, where the gravity data appear to be inconsistent with the geology of the central uplift (CU). The main problem with these previous studies was that they compared the negative anomaly over the granite to the surrounding sedimentary rocks. Additionally, results from recent geological mapping activities suggest a more complex geology in the central portion of Araguainha, indicated by the presence of phyllites as part of the basement rocks, as well as the extent and distribution of breccias, suggesting the need for new geological e geophysical models (Crósta et al. 2019).

In the present manuscript, the result of 3-D gravity modeling for the Araguainha impact structure is addressed, focusing on the central uplift and based on data collected from over 300 new ground stations in its central area. Additionally, to shed light on the CU's formation. The results of the gravity modeling were compared with those of the numerical modeling in terms of morphometry and pressure regime. These results led to a better understanding of the highly deformed sedimentary strata surrounding the central basement (granite plus phyllite).

GEOLOGICAL SETTING

The Araguainha impact structure is the largest and, likely the oldest known impact structure in South America, with a diameter of 40 km and an area of about 1300 km², formed approximately 253 Mya. (Crósta 1982, Tohver et al. 2012, Erickson et al. 2017, Crósta et al. 2019, Hauser et al. 2019). It is located on the boundary between the states of Goiás and Mato Grosso, Brazil, centered on the coordinates 16°47'S and 52°59'W. The structure

was formed in the northeastern part of the Paraná Basin and comprises sedimentary supracrustal rocks and a basement composed of igneous and metamorphic rocks. The radiometric age of these basement rocks ranges between 700 and 450 Ma. (Cordani et al. 1984). The Paraná Basin's lithological record is comprised of sedimentary and volcanic rocks, with ages ranging from Neo-Ordovician to Neo-Cretacean (Milani et al. 2007, Pereira et al. 2012).

The morpho-structural zones of the Araguainha impact structure comprise, from the center outwards, the central peak within a radius of ~2.5 km from the center, the annular basin from 2.5 km to 8 km, at least two concentric inner rings at ~11 km and ~16 km, and the crater rim at ~20 km (Lana et al. 2007, 2008, Yokoyama et al. 2012, Hippert et al. 2014).

The geological units exposed at the structure are the Serra Negra granite surrounded by the sedimentary sequences of the Paraná Basin comprising, from the lower one to the upper units, the Furnas, Ponta Grossa (both Devonian), Aquidauana (Carboniferous) and the Passa Dois Group (Permian) (Fig. 1), all of them forming concentric rings around the CU, composing an overall bull's eye pattern for the local geology.

The Serra Negra granite resulted from post-Brasiliano intrusive magmatic events that occurred from 600 to 500 Ma. (Brito Neves et al. 2014) and, in terms of texture and composition, they have been related to the São Vicente granite that occurs in nearby locations in Mato Grosso

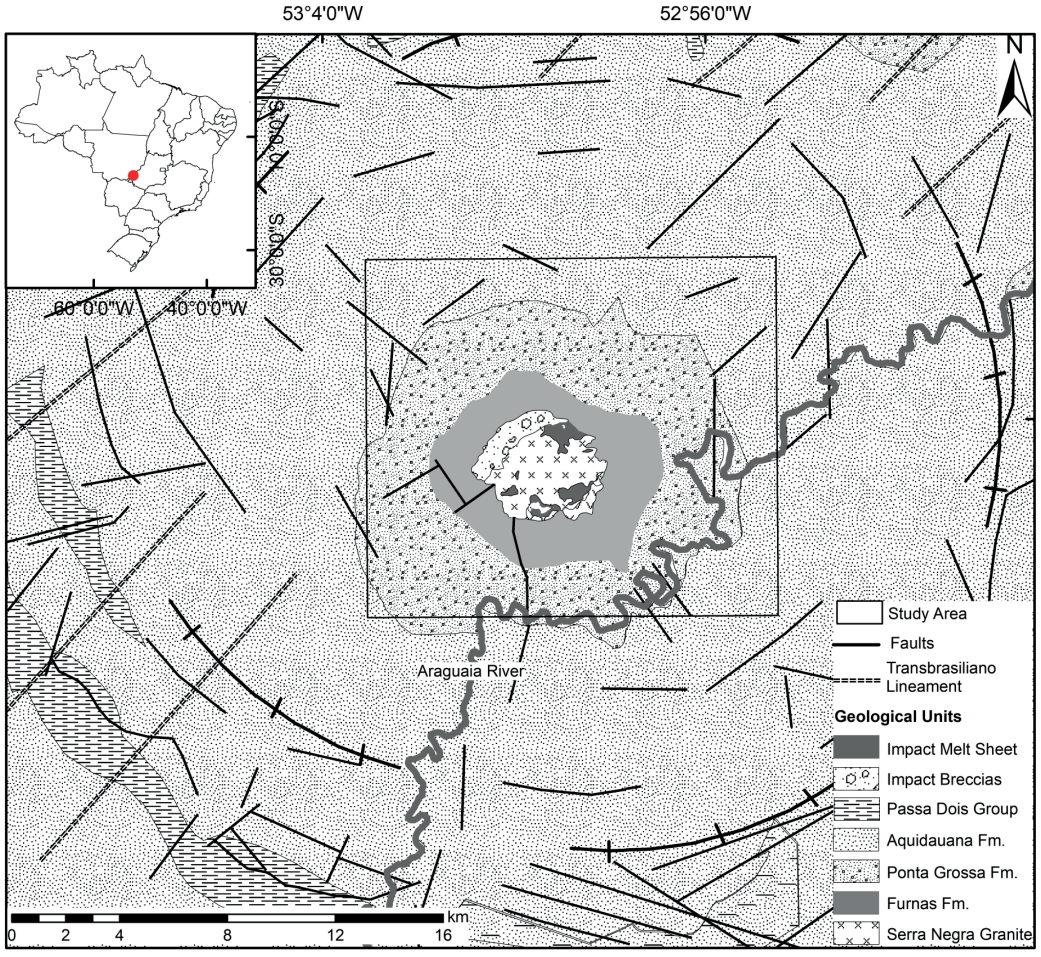

Figure 1. Simplified geological map of the Araguainha impact structure (after Lacerda Filho et al. 2004). The central square depicts the location of the study area, where data were collected from gravity stations.

state (Godoy et al. 2010). The contact between the crystalline core and the supracrustal Paleozoic strata (Fig. 1) is characterized by shock deformation (melting, faulting, fracturing, brecciation), resulting from the uplift of basement rocks (Lana et al. 2007). The basement rocks outcrop in an area ~5 km wide and consists of partially shocked and melted alkali granite, sometimes exhibiting porphyritic textures, and syenites, and of similarly shocked phyllites related to the Cuiabá Group (Yokoyama et al. 2012). Evidences of three metamorphic phases are mentioned by Crósta et al. (2019), the first related to the Brasiliano-Pan Africano cycle, the second related to the intrusion of the granite, and the last one, to the metamorphism caused by the impact. Shatter cones are usually found in phyllites of the Cuiabá Group, mainly in the contact between them and the granites (Crósta 1982, Engelhardt et al. 1992, Lana et al. 2008).

The collar surrounding the CU is characterized by concentric and radial ridges, predominantly composed of white sandstones and microconglomerates of the Furnas Formation. Both lithologies, the granite and metasedimentary rocks, as well as the surrounding Paleozoic sedimentary units, exhibit a predominantly outwards slope, as shown in geological profile presented by Lana et al. (2007, fig. 1). There are patchy exposures of polymictic impact breccias between the core and this collar, including some suevites (clast-bearing impact melt breccias) (Yokoyama et al. 2012).

The Furnas Formation is composed of a succession of white quartz sandstones with various stratifications, and of conglomerates, silt lenses and shales (Milani et al. 2007, Pereira et al. 2012). It shows an annular shape with a maximum width of ~2.5 km to a maximum of 6 km and an average of 11 km from the center. The whole unit is folded, with high dip angles (Yokoyama et al. 2012, Crósta et al. 2019). Hippert et al. (2014) report on the large-scale folds and microscopic brecciation exhibited by the Furnas sandstones, resulting from rock strength degradation triggered by the shock waves following the impact. These authors pointed out that the heating and decompression experienced by these rocks led to vaporizations and expansion of fluids in the sandstone pores, increasing the brecciation by liquefying the rocks and allowing for the chaotic folding pattern at scales of blocks up to 100 m in length in the CU. They argue that this vaporization-assisted microbrecciation may have inhibited the formation of pseudotachylites and that, in general, impact-induced liquefaction of sedimentary rocks depends on the presence of fluids filling in the pores and the occurrence of related microbrecciation, which in sufficient amounts would dissipate most of the impact energy.

The Ponta Grossa Formation is composed of shales and sandstones (Pereira et al. 2012), and is found in between the Furnas and the the Aquidauana formations in the annular depression. It is composed of glacial diamictites and fining-upward sandstones, reaching the level of turbidite deposits (Milani et al. 2007, Pereira et al. 2012). Both units have concentric and radial faults in the annular depression of the impact structure (Crósta 1982).

The units of the Passa Dois Group are composed of shales, pelites, claystones and sandstones found in the elevated areas of the structure's outer rim, which correspond to the remaining ridges of semicircular grabens (Maranhão & Petri 1996, Crósta 1999, Milani et al. 2007, Pereira et al. 2012).

The CU, which is the focus of this study, is composed of porphyritic granites at the innermost portion of the structure, associated with phyllites and metasandstones from the

Cuiabá Group in the southeastern area, partially surrounded by polymict impact breccias (Engelhardt et al. 1992, Lana et al. 2006, 2007, 2008, Hauser et al. 2019) and highly deformed rocks of the Furnas and Ponta Grossa formations (Figure 1). Silva et al. (2016) classified the impact breccias as melted lenses and melted veins.

GEOPHYSICAL CONSTRAINTS

The first geophysical studies on the Araguainha impact structure were carried out as part of the Alto Garças Project in the 1970s, that acquired aerial gamma-ray spectrometric and magnetic data. The data obtained through this project indicated circular and concentric anomalies associated with the Araguainha structure, especially high potassium levels at the center of the structure, coinciding with the granite exposures. The magnetic data indicated that the top of the basement lies at depths of 1500 m to 1700 m, and becomes progressively shallower towards the center. The pattern of the magnetic anomaly indicates conspicuous NE-SW lineaments related to the Transbrasiliano Lineament (Crósta et al. 2019). Masero et al. (1994) used magnetotelluric data to estimate the depth of the crystalline basement under the Araguainha structure's CU. According to these authors, the basement consists of a well-defined annular formation with about 1000 m depth and 9 to 20 km radius. Masero et al. (1997) built 2D and 3D magnetotelluric models that suggest the existence of an elliptical deformation due to low resistivity at shallower depths, possibly caused by the fractures in the granitic rocks. Schnegg & Fontes (2002) confirmed the existence of a 4-km-wide conductive source at 1-2 km depth, based on their interpretation of the magnetotelluric data. The presence of this conductive source was also supported by Vasconcelos (2007), who analyzed the aeromagnetic data's power spectrum. The amplitude of the magnetic data's total gradient shows a well-marked area with high values coinciding with the granite at the CU. This later author also pointed out the intriguing gravity signature of Araguainha, as the granite has a negative gravity anomaly in comparison with the sedimentary sequences surrounding it (Furnas and Ponta Grossa formations), which is inconsistent with the signature expected for these types of lithologies. Tong et al. (2010) carried out an electrical survey and identified rocks with different physical properties within the granite, which they interpreted as being related to the occurrence of polymictic breccias. Additionally, the low resistivity values in this area were interpreted as heterogeneities of the polymictic breccia matrix, characterized by higher porosity due to micro-fracturing, as previously described by Engelhardt et al. (1992).

METHODOLOGY

Gravity modeling

The gravity data were collected during two field campaigns using a differential gravity meter (Scintrex CG-5), with a standard resolution of ~1 μGal and a standard deviation of ~5 μGal. A total of 328 stations spaced 230 m apart, on average, were measured. The stations were spread throughout the structure, with a tighter spacing of ~200 m in the first 10 km radius from the center (Figure 2), the most complex region and the focus of our 3D modeling.

Absolute gravity values were obtained from the differential measurements using a reference station located in the nearby town of Alto Araguaia. We have also corrected the data for dynamic and static drifts of the gravity meter using that reference station (e.g., Jacoby & Smilde 2009). The gravity meter automatically

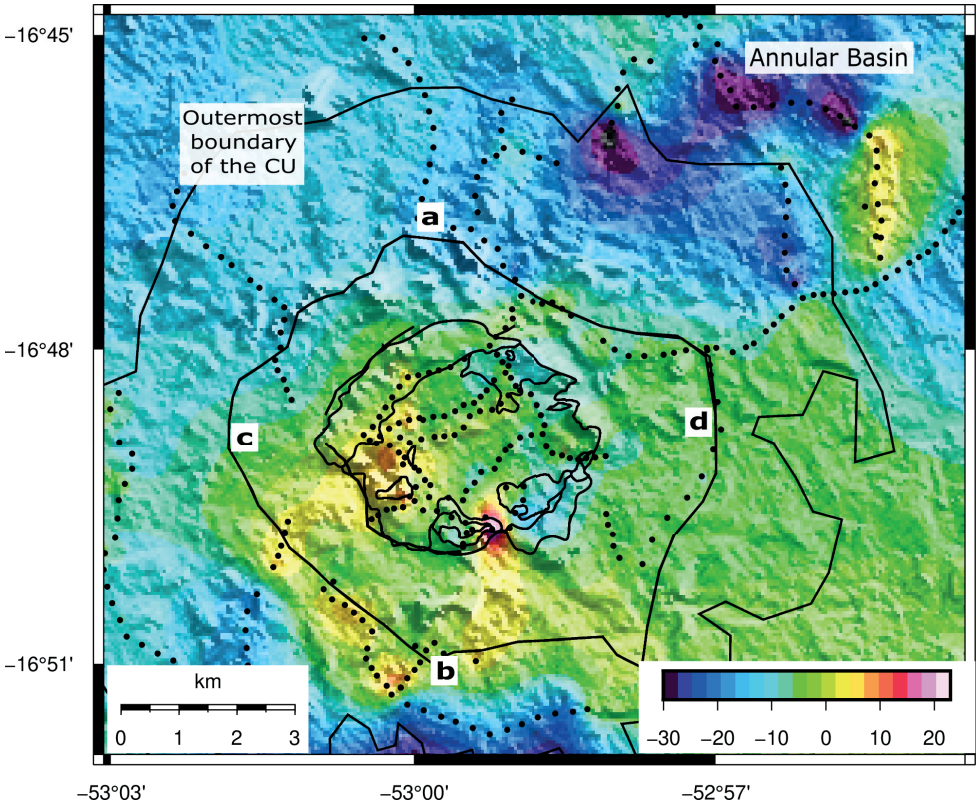

Figure 2. Residual Bouguer anomaly map of the Araguainha impact structure's center, showing the 300+ gravity stations from which the data was collected. Color scale is in mGal. Stations are closest to each other at the center of the structure. Thin black lines correspond, from the innermost to the outermost, to: granite, Furnas Formation, and Ponta Grossa Formation, respectively. All of them comprise the central uplift. Ends of profiles A-B and C-D are indicated on the map.

corrected the measurements for the Earth tide effect using the classic Longman's formula.

Horizontal and vertical coordinates were acquired with a ProXT differential GPS. Differential corrections were applied using a nearby reference GPS station, resulting in coordinate accuracies of ~50 cm. The reader is referred to Li & Götze (2001) for a discussion about the importance of using ellipsoid heights in the calculations of gravity anomalies, when possible.

Bouguer anomalies were calculated using a reduction density value of 2.67 g.cm^{-3}, which is a standard value corresponding to the global average density of the continental crust. Although the densities of the study area are lower, using a lower value for the gravity reduction did not result in a significant difference in the residual Bouguer anomalies. The theoretical gravity at all locations was calculated using the GRS80 reference ellipsoid.

The data were interpolated in a regular 79 × 70-point grid with 200 m of distance between points, using the minimum curvature algorithm (Briggs 1974). A regional-residual separation was carried out to remove regional trends. The regional field was calculated by an upward continuation to 1 km of the total Bouguer anomaly grid.

A three-dimensional mass density model was obtained from the residual Bouguer anomalies by applying the inversion method implemented in the VOXI Earth Modeling tool of Oasis Montaj™ (Geosoft 2016). A similar approach was employed by Giacomini et al. (2017) and the details of the theoretical formulation of this method is presented in Li & Oldenburg (1998).

Given a set of gravity anomalies $d = (d1, d2,..., dN)^T$ for N observational points, and a set of density contrasts $p = (p1, p2,..., PM)^T$ for M subsurface regular blocks, these two vectors are connected by a linear system, $d = Gd$, where G is

known as the sensitivity matrix. The inversion is formulated as an optimization problem where a global objective function Φ is minimized, subject to matrix constraints. The objective function consists of the weighted sum of a model-fitting function (Φm) and an error-fitting function between observations and predictions (Φd), with the objective of finding $\Phi = \Phi d + \beta \Phi m$, subject to $pl \leq p \leq pu$, where pl and pu are the lower and upper bounds of the density contrast, and β is a parameter that controls the relative importance of Φm.

In addition to the upper and lower density bounds, this inversion procedure requires a density reference model as another constraint. We used representative density values of the main lithotypes in the Araguainha area to fill this reference model (Vasconcelos 2007, Yokoyama et al. 2012). These densities range from 2.1 g.cm^{-3} to 2.45 g.cm^{-3}, with the lowest values corresponding to the shales of the Irati Formation and the highest to the granite. The average density is 2.35 g.cm^{-3}. The reference model was also built based on the granite geometry proposed by Masero et al. (1994, 1997). It is defined by a symmetrical ring with a ~9 km radius at a depth of about 1000 m in the granite. The reference model was built considering the following densities: (i) 2.45 g.cm^{-3} for rocks at depths of over 1000 m, (ii) 2.1 g.cm^{-3} to 2.45 g.cm^{-3} for rocks at depths of 500-1000 m, and (iii) 2.1 g.cm^{-3} for rocks at depths shallower than 500 m, except in the case of granite outcrops, for which a density of 2.45 g.cm^{-3} was considered. A SRTM image with a maximum resolution of 150 m was used as the topographic surface.

Numerical modeling of the impact

For the numerical modeling of the impact and to assess the subsequent formation of the structure, we used the iSALE-2D shock physics code (Wünnemann et al. 2006), which is based on the SALE hydrocode (Amsden et al. 1980). In order to simulate hypervelocity impacts on solid material, SALE was modified to include an elastic-plastic constitutive model, a fragmentation model, and a sophisticated equation of state (ANEoS, Thompson & Lauson 1972), including multiple materials (Melosh et al. 1992, Ivanov et al. 1997). More recent improvements have also included a modified strength model (Collins et al. 2004) and a porosity compaction model (Wünnemann et al. 2006, Collins et al. 2012). Due to resolution limitations, petrophysical variations between different sedimentary units could not be considered in our model. We simplified the target to comprise only two layers, one representing a single unified sedimentary layer and the other representing the crystalline basement. The sedimentary units extend to a depth of ~1850 m, and all layers were assumed to be homogeneous. They were represented by quartzite materials using a ~10% porosity model (Wünnemann et al. 2006) to calculate the Bouguer anomaly and to compare it with the observed Bouguer anomaly.

A granitic composition was assumed for the impactor to reduce the number of different materials in the model, as in the crater formation mechanism only the impactor's mass matters. The impactor consisted of 20 computational cells spread across its radius (20 CPPR). All material properties and parameters are listed in Table I. We considered vertical impacts only, which is enforced by the 2D cylindrical symmetry of the computational mesh. To represent the most frequent impact angle of 45 degrees in the 3D model, we assumed only the vertical component of the velocity vector as impact speed, as suggested by Chapman & McKinnon (1986) and Elbeshausen et al. (2009). In the models, the impact occurred at a speed of 12 km/s, which is equivalent to a vertical velocity component of 17

Table I. Parameters of the best fitting numerical model of the Araguainha impact structure.

PARAMETERS	ASSUMPTIONS
Impactor: Diameter Impact velocity Material/EOS Density	 3000 m 12 $km.s^{-1}$ granite/ANEOS 2.65 $g.cm^{-3}$
Upper sedimentary layers Material/EOS Cohesion C_s Dry friction coefficient ϕ_S Thickness	Quartzite/ANEOS Intact Damaged 1 MPa 0.01 MPa 2.0 0.01 1750 m
Granitic Basement Material/EOS Cohesion C_B Dry friction coefficient ϕ_B	Granite/ANEOS Intact (Y_0) Damaged (Y_{d0}) 10 MPa 1 KPa 2.0 (FricInt) 0.6 (FricDam)
Model setup Number of cells nx x ny (radial, vertical) Spatial increment (high resolution area) Resolution in cells per projectile radius (CPPR)	 300 x 330 cells (high res. zone) 60 m 10
Acoustic fluidization parameters *Dimensionless Acfl. fluidized viscosity g_h *Dimensionless Acfl. acoustically fluidized decay time g_b	Granite Sedimentary rocks 0.01 0.0008 115 150

*** Dimensionless parameters were calculated according to Wünnemann & Ivanov (2003), assuming a speed of sound of 5000 m/s. Acfl = acoustically fluidized.**

km/s, the average terrestrial impact speed (e.g., Ivanov 2001), with a horizontal 45-degree angle.

The thermodynamic behavior of the target rocks was modeled using the Analytic Equation of a State (AnEoS, Thompson & Lauson 1972) for granite (Pierazzo et al. 1997) and quartz (Melosh 2007). Due to the similarities between sedimentary layers, we simulated the thermodynamic behavior of all of them using ANEOS for quartz. The rocks' ductile and brittle mechanical responses to large deviatoric stresses, including dynamic fracturing, were calculated using the constitutive model developed by Collins et al. (2004). In this model, the yield strength [Y] is a function of pressure [P], temperature [T] and deformation history (damage). The main parameters describing the resistance of rocks against shear deformation are given by coefficients of internal friction [ϕ] and cohesion [C_s] for pristine (intact, subscript i) and heavily fractured or brecciated (damaged, subscript d) rocks, respectively. The standard values of [ϕ] and [Y_0] for the granitic basement rocks were based on the strength data for Westerly granite (Collins et al. 2004, Table I). In contrast, it was not possible to reproduce the deformation of the sedimentary units with standard sandstone parameters. Instead, [ϕ] and [Y_0] for the sedimentary unit in a fully damaged state were treated as free parameters to fit the

observed structure. An extensive study of the parameters revealed very low values (ϕ_d = 0.01, Y_{d0} = 0.01 MPa) compared to those of typical sandstone. The implications of such low effective strength will be discussed later, but it may be justified as a consequence of water saturation and/or the presence of planes of weakness (slip planes) within the sedimentary strata. Finally, we also assumed temporary weakening of the basement rocks during the crater's formation due to acoustic fluidization (Melosh 1979, Melosh & Ivanov 1999, Wünnemann & Ivanov 2003). The acoustic fluidization parameters were chosen within the range suggested by Wünnemann & Ivanov (2003).

RESULTS AND DISCUSSION

Bouguer anomaly and 3D gravity model

The residual Bouguer anomaly map for the CU does not show a circular pattern which is typically observed in impact structures (Figure 2). However, contrary to the uniform circular low-gravity signature over the granite presented by Vasconcelos (2007), our results show variations in the gravity field, with some local highs. In terms of absolute Bouguer values, those found for Araguainha were different than the ones expected for an impact structure of this size. Considering the relationship between crater diameter and gravity amplitude, proposed by Pilkington & Grieve (1992), the gravity anomaly expected for a 40-km-size crater would be –20 mGal, which is ~10-20 times the anomaly observed over the center of Araguainha. According to Grieve & Pilkington (1996), this may be explained by the fact that the structure is not pristine, and has undergone approximately 300 m of erosion (Lana et al. 2007). The ~40 km-wide St. Martin impact structure in Canada has also an uplifted granitic center, with rocks of the crystalline basement exposed in the inner part. The crater's cavity was filled with breccias formed by impact and post-impact sediments (Bannatyne & McCabe 1984). The similarity can be seen in the St. Martin residual Bouguer anomaly map, which shows a uniform low -gravity signature in the CU, attributed to the fracturing of basement rocks (Zivkovic 2012), as can be observed in Araguainha structure. There are other structures with characteristics akin to those of Araguainha in relation to the size, age, and geological context of the target rocks. Structures formed in crystalline basements generally have positive anomalies in the CU's region, such as the 70 km-diameter Morokweng impact structure, formed on Archean granitoids, the aero-gravimetric data of which features an elliptical concentric ring structure, with a negative anomaly in the granites due to the fracturing of rocks (Henkel et al. 2002, Andreoli et al. 2007).

The highest Bouguer anomaly values are found in areas of granite outcrops and in the area corresponding to the Furnas Formation's sedimentary rocks. The former show alternance of highly positive (5.0 to 7.1 mGal) and negative values (-5.0 to -0.9 mGal), which roughly coincide with Engelhardt et al.'s (1992) description of breccias and lenses of melted materials. The negative values are in agreement with the description of cataclasite bands within the granite (Yokoyama et al. 2012), and with the observation of intensely fractured granites based on scanning electron microprobe studies of shock veins (Machado et al. 2008). This intensely fractured granites form a partial ring, with anomalies ranging between 5.0 mGal and 7.1 mGal (Figure 2). In this sense, there is an apparent similarity between both signatures: the positive peaks of the granitic area and the Furnas Formation, which is unusual as sedimentary rocks are less dense than granites. The reason for the anomalies in the

Furnas Formation may be related to a certain thickening of sedimentary rocks in the CU. This effect was described by Lana et al. (2008) as a possible result of mass movements during the impact, based on field observation of several Furnas sandstone in topographic peaks around the granite.

We run the gravity inversion algorithm several times using the residual Bouguer anomaly shown in Figure 2 as input data, as well as upper/lower bounds and absolute values of densities as constraints (see Gravity inversion section). We then selected the inverted 3D density model that is more consistent with the known geology of the area and performed: (i) a general analysis based on tridimensional blocks, (ii) a more detailed analysis based on profiles.

The 3D model was roughly discretized in three different density units: 2.1, 2.2-2.3 and 2.45 g.cm^{-3} (Figure 3). Figure 3a shows all units in a

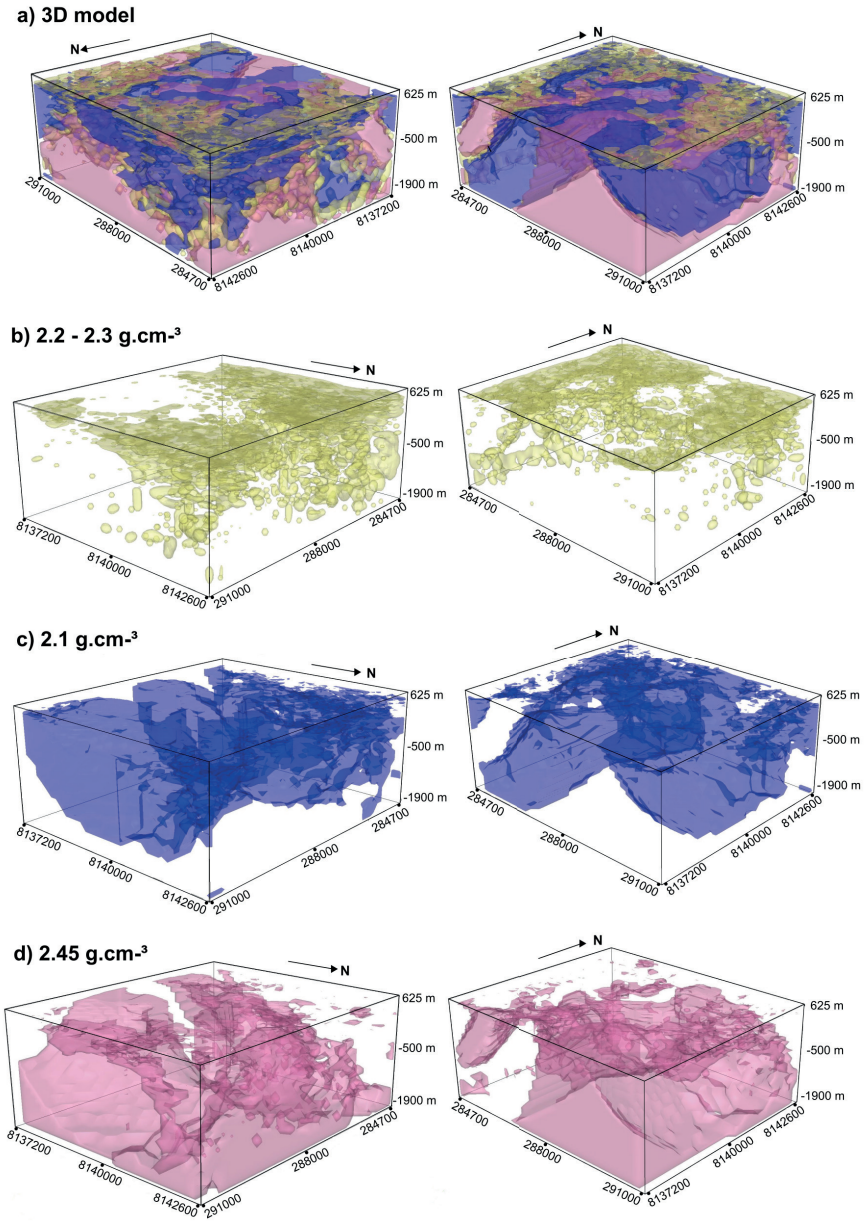

Figure 3. 3D gravity inversion model of the central uplift. (a) Complete model. From top to base: (b) Intermediate density sources (2.2 - 2.3 g/cm^3), likely where breccias and sandstones of the Furnas Formation occur. (c) Low density sources (~2.1 g/cm^3), mostly located beneath the top block, and possibly related to sandstones of the Furnas Formation and/or to highly-cracked granites at the center. (d) High-density sources (~2.4 g/cm^3) representing the granites. This bottom block extends outward, beneath the Furnas Formation, as mentioned in the text.

single plot, and Figures 3b-c depict the location of each unit separately. The first unit (Figure 3b) corresponds to regions where the residual Bouguer anomaly is lower (between −0.5 mGal and −2.7 mGal), as shown in Figure 2. This unit is generally located at shallower depths, and may be interpreted as the Furnas Formation. This is supported by the fact that it outcrops in some areas which fall within this range of values. The next unit represents mass sources with 2.1 g.cm^{-3} density, and is located ~500 m below the ground floor (Figure 3c), being composed of low-density sources (in blue) located within a larger high-density unit (in pink). According to field observations, it might correspond to the brecciated and heavily fractured granites with veins, to the breccias at the borders of the granite, and to an intensely fractured granite in the deeper region. A high-density unit (2.45 g.cm^{-3}) was found at the surface, extending across the whole study area, at depths greater than 1000 m (Figure 3c). This high-density unit occurs in the areas closest to the center of the structure. Although the units do not have well-defined lithological boundaries, the model is in agreement with what is expected for the geology of the region.

The 2D profiles presented in Figure 4 correspond to the sections extracted from the 3D model that cross the central area both, N-S and E-W sections (see Figure 2 for the profiles' location). The two gravity profiles were chosen

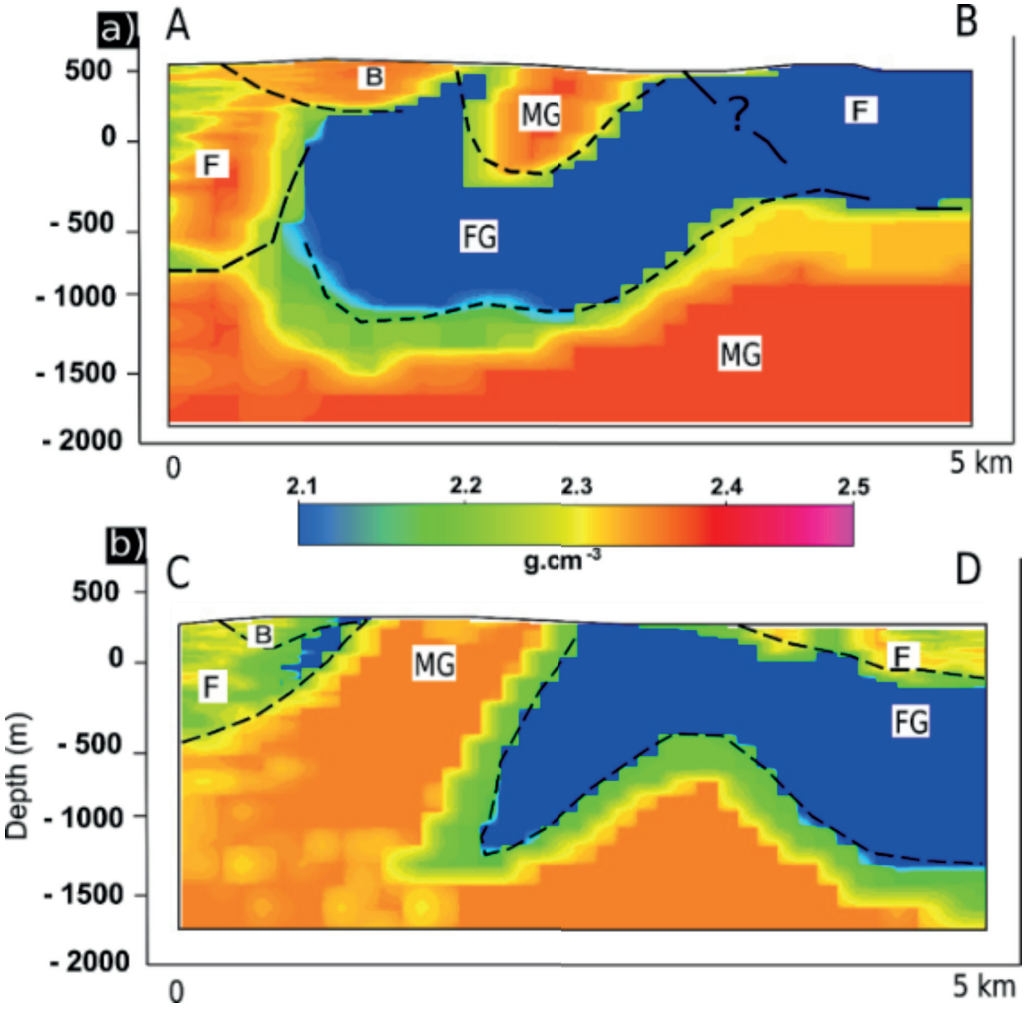

Figure 4. Sections obtained from the gravity inversion, detailing the area of the central granite. (a) N-S profile, (b) E-W profile. The location of both profiles is shown in Figure 2. B – Polymictic breccias/Melts, F – Furnas Fm., MG – Massive porphyritic granite, FG – Fractured granite. Dashed lines mark high density contrasts and are associated with the changes in geology.

because they capture the highs and lows of the residual Bouguer anomaly within the center of the structure and depict the complexity of the gravity model. They show at least three different density values, which were used to better understand the distribution of densities within the granite based on their locations. The N-S profile (A-B) shows that densities varying between 2.4 g.cm^{-3} and 2.5 g.cm^{-3} can be assigned to different lithological units separated by black dashed lines. At ~1000 m depth, the "MG" unit (Massive porphyritic granite) extends over the entire profile. This same lithology also occurs at the center, where the granites outcrop, almost coming into contact with the breccias ("B" in Figure 4a). Underneath the granite, the model shows an elongated area with low density (2.1 g.cm^{-3}) between ~500 and ~1000 m- depths ("FG" in Figure 4). This unit may correspond to the fractured and brecciated granites, which would explain the low gravity in this area, as shown in Figure 2. Although they cannot be distinguished by density, these rocks also contain slivers of melt, as described by Yokoyama et al. (2012). In the southern part of the profile, the inversion algorithm was unable to distinguish between the Furnas Formation ("F" in Figure 4a) and the FG unit, due the lack of stations in this area. The C-D profile shows sources with densities varying between 2.2 and 2.3 g.cm^{-3} at the rim of the central granitic region, which may correspond to breccias and the Furnas Formation ("B" and "F" in Figure 4b, respectively). At the center, there is a low-density source (~2.1 g.cm^{-3}) ("FG" in Figure 4). Considering that the granite outcrops in this central area, this same low-density source may correspond to the fractured granite dipping outward, below the Furnas Formation's sandstones. The section also contains a source with ~2.3 to 2.4 g.cm^{-3} density dipping westward, corresponding to the granite ("MG" in Figure 4b), the contact of which with the fractured granite is irregular. This source apparently showed up at over 1.5 km depth and may represent the depth of the original basement. Analyses of this crater's basement show an irregular surface that is in contact with the sedimentary rocks of a multi-ringed basin, found at the same depth as the body with 2.5 g.cm^{-3} density. The study area's outermost limit features units with medium to low densities, ranging from 2.25 g.cm^{-3} to 2.1 g.cm^{-3}, which may correspond to the areas where the Furnas Formation's rocks and polymictic breccias outcrop. As bodies with 2.1 g.cm^{-3} density occur in the granite's innermost area, it is not possible to estimate contacts only considering the density distribution.

All these results show that the area that belongs to the granite also contains blocks with other densities, indicating the presence of fractured granites, breccias and even sandstones. This assumption shows the granite's internal heterogeneity, which is likely responsible for the low Bouguer anomaly. Corroborating our hypothesis, Masero et al. (1997) and Tong et al. (2010) demonstrated that the resistivity in the granitic area is significantly lower, suggesting that the upper crust's fractures were induced by the impact.

Numerical model of the impact

The model quantified the uplift and the extent of the zone with heavily fractured rocks. The best match between the model and the real structure was achieved with a 3 km-diameter spherical impactor, assuming an impact speed of 12 km.s^{-1}. Different stages of the crater's formation were represented in the best fitting model, the numerical model also showed how the target rocks were affected by the impact. Additionally, we used this information to support the gravity analysis and understand the nature of the contact between the granite and the surrounding sedimentary rocks.

Figure 5 shows the main stages of the crater's formation. At about 15 s, the transient crater with a diameter of 16 km and a maximum depth of ~7 km was formed (Fig. 5a). The transient crater was unstable in relation to the gravity field, collapsing shortly after. The formation of the central peak started 30 s after the impact (Fig. 5b), and the crater's diameter continued to grow due to inward slumping of the rim. After 90s, the crystalline basement's rocks rose up

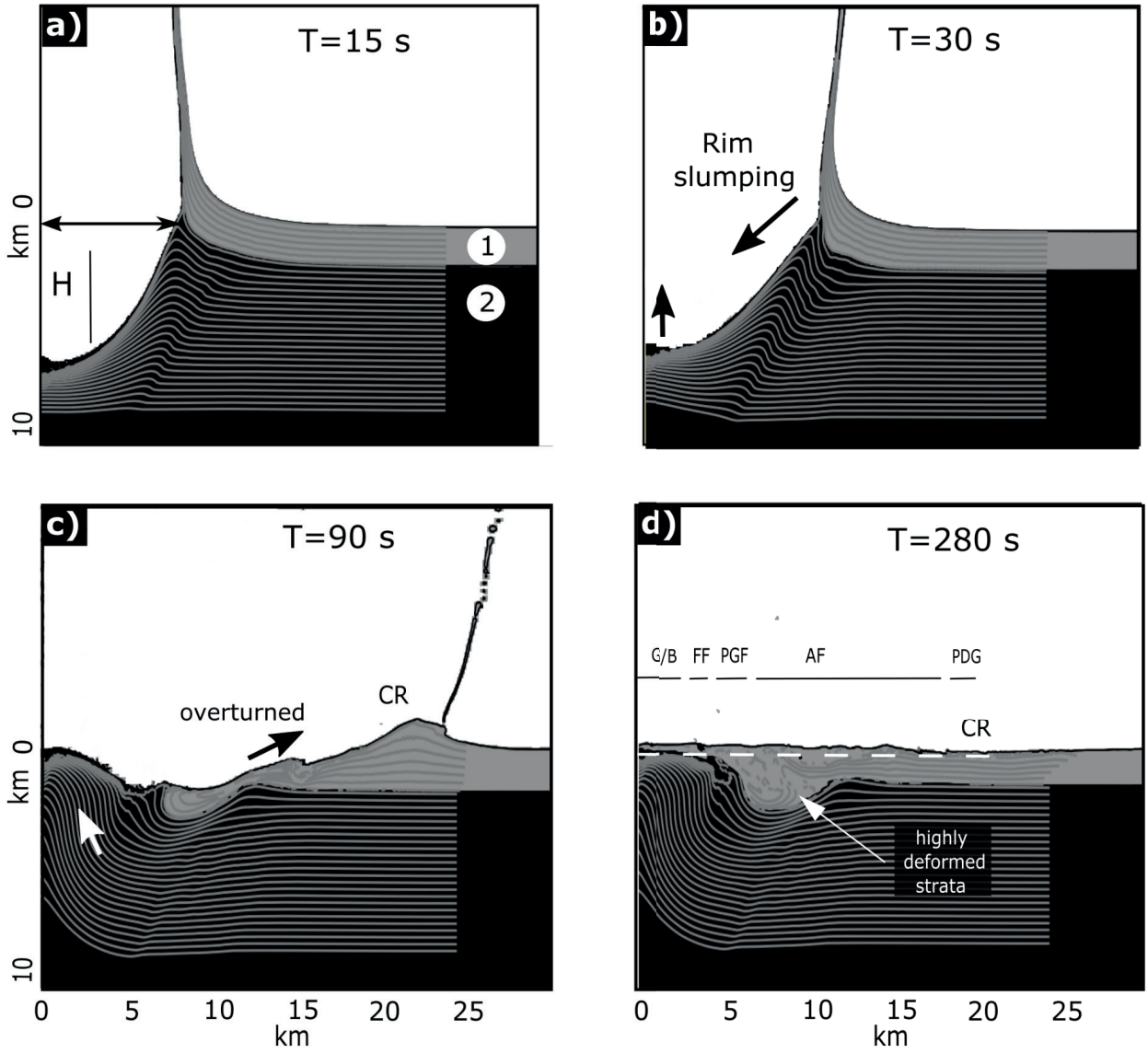

Figure 5. Best-fitting model for the impact event, showing the right-hand side of the model. (a) 15 sec after the impact, the crater reaches ~16 km diameter and ~7 km depth. (b) After 30 s, the formation of the central uplift begins. (c) The basement rises and remains exposed after 90 sec. (d) After 280 s, the structure reaches gravitational stability. CR = crater's rim. Number 1 corresponds to sedimentary rocks, and number 2 to the granitic basement. The solid tracer lines connect the positions of the tracer particles that marked the center of each computational cell at the beginning of the simulation, following the paths of the material in that cell. Where the separation between tracer particles that were originally horizontally adjacent to each other exceeds ten times the initial separation (250 m), there is no line connecting these points. The extreme deformation in the sedimentary collar around the central uplift is highlighted by folding and discontinuities in the tracer lines at radial distances of 5-15 km. A similar deformation is observed in the real strata of the Furnas Formation.

to the original ground level, becoming exposed (Fig. 5c). The ejecta curtain consisting entirely of sedimentary material was still suspended in the air, with a radial distance of approximately 20 km. Simultaneously, a thin layer of sedimentary strata moved inward, covering the basement granite and abutting onto the flank of the rising central peak, subsequently, the sedimentary rocks rotated into a vertical attitude, and then overturned. This is consistent with the occurrence of overturned layers of sedimentary strata at the flank of the central peak, as described by Lana et al. (2008). After about 100 s, the ejecta curtain collapsed onto the crater's rim. After 280 s, the main dynamic motions ceased, and the crater reached gravitational stability, with flat attitude of the uppermost sedimentary strata (Fig. 5d) and basement rocks uplifted by ~2 km. Due to the rock flow, a gentle topographic relief characterized the crater's final geomorphological setting. In this model, the radius of the gentle topographic gradient is ~20 km, and may be interpreted as the crater's rim, as proposed by Crósta (1982) and Lana et al. (2007). The final results showed that the granitic basement was covered by the thin sedimentary package in the past. Considering 250-300 m of erosion, as estimated by Lana et al. (2007), the model showed that the currently exposed granitic basement would be ~4-6 km wide, in accordance with the actual ~5 km exposure shown in Fig. 2. The right-hand frame of the last image shows curved lines, which represent strata that was strongly deformed by the impact (Fig. 5d), being in agreement with Lana et al.'s (2007) description of the Furnas Formation's actual strata.

The model allows us to corroborate some of the assumptions made above. Firstly, the diameter of the uplifted area is ~16 km, which is apparently broader than the granite's 6 km diameter. However, Crósta (1982, 1999), Lana et al. (2007, 2008) assumed that the CU's area is composed of the granite and the Furnas and Ponta Grossa formations (Figure 1), which is in agreement with our results. This analysis implies that the rocks of the Furnas and Ponta Grossa formations were uplifted along with the granitic basement. Therefore, the presence of the basement beneath these sedimentary rocks is very likely responsible for the high positive Bouguer anomaly found in these areas, as described above. This can be better understood by noting that the granite is dipping outwards within ~5-6 km of radial distance from the center (Figure 5d), which was also observed by Masero et al. (1994) through magnetotelluric data. Secondly, our model shows that the rocks at the center were subjected to temperatures of ~ 1500 K, and the most affected ones are found in the first 2 km of depth (Figure 6a), which coincides with the thickness of the package shown by our gravity models with breccias and molten rocks. The Bouguer anomaly obtained by the porosity model shows a positive outward trend (Figure 6a – dashed line), which roughly coincides with the real Bouguer anomaly (Figure 6a – black line), depicted in Figure 2. The molten rocks and breccias may have contributed to the Bouguer anomaly's reduction of the granite, which is an expected effect. Finally, our model shows that the peak pressure reached over 50 GPa after 0.5 s, decreasing to ~15 GPa at the center of the crater in the first 1 s (Figure 6b). The pressure peak is roughly consistent with the maximum pressure of 40 GPa estimated based on petrography studies of PDFs found in zircons (Hauser et al. 2014).

Thus, the unusual and variable Bouguer values over the granite's area might be explained by the following hypotheses:

(i) The presence of low-density materials resulted from the mechanical crushing and large-scale fracturing of the basement. The numerical models developed by Collins (2014)

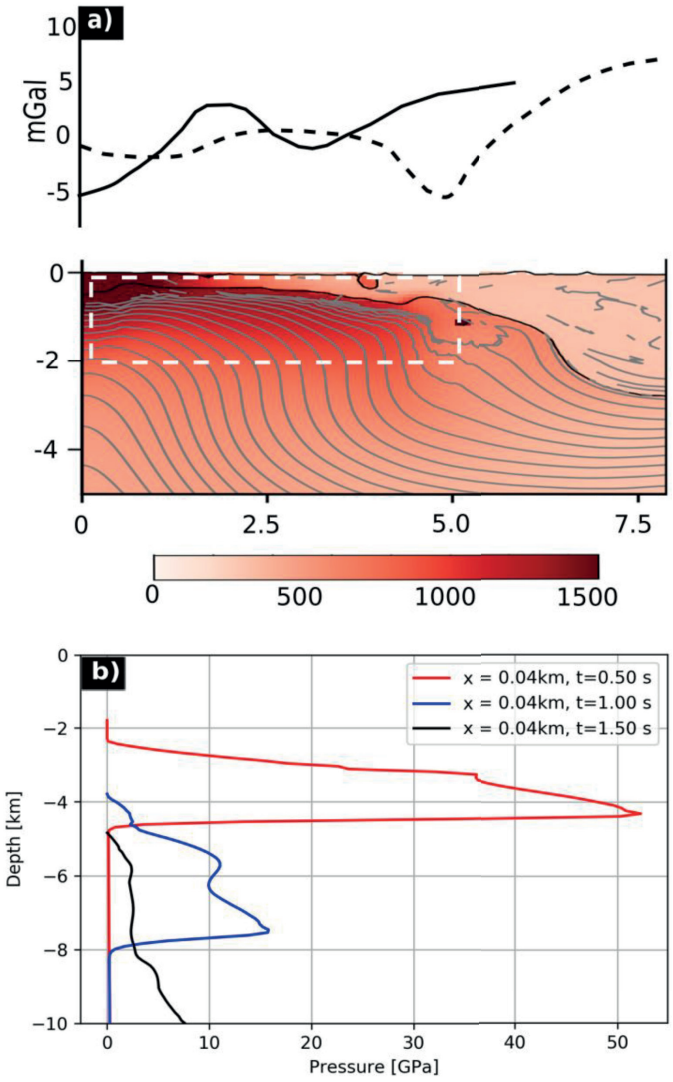

Figure 6. (a) Last timeframe obtained by iSALE showing the temperature range (in K) within a 7.5 km radius. The dashed white line corresponds to the same area (5 km x 2 km) of the gravity inversion presented in Figure 4. The temperature peaks in this area are likely related to the formation of melts in the granite. The upper figure shows the Bouguer anomaly estimated by the porosity model (dashed line) and the real Bouguer anomaly obtained from Figure 2 in the E-W direction. (b) Linear downward pressure trend at the innermost center. The pressure peak is around 53 GPa after 0.5 s, falling to 15 GPa after 1 s, and to less than 10 GPa after 1.5 s.

with dilatancy show that the fracturing induced by an impact progressively increases the porosity of rocks, which might be reflected by the Bouguer anomaly. This is consistent with the low -resistivity data obtained by Tong et al. (2010) using geoelectric techniques. Additionally, Schnegg & Fontes (2002) used electromagnetic depth sounding (MT) to suggest a conductive source with ~1 km of depth and 4 km of width at the center of the structure. Water-filled fractures and pores may indeed explain high conductivity, which supports the proposed depth of the low-density gravity anomaly presented here,

(ii) The interaction of the target rocks with water. The numerical models show temperatures as high as thousands of degrees that were likely responsible for the generation of the molten portions of the granite, as observed in the field (Lana et al. 2007, Machado et al. 2008). Similar results have already been described for other impact structures due to the interaction of molten rocks with sea water (Grieve et al. 2010). This interaction might also have happened in Araguainha because it was formed in a shallow sea depositional environment (younger Permian sequences that occur at the edge of the structure) where there was a thin water layer at

the surface. Additionally, the low-density zone in the gravity model roughly coincides with the heated zone in the numerical model (~1500 K ≈ 1200°C). This temperature corresponds to the lower limit of thermal origin of molten rocks, similarly to magmatic rocks (e.g., Carpozen et al. 2005, Koch et al. 2012, Eitel et al. 2014), and is associated with peak pressures of 50-80 GPa (Grieve et al. 1977).

CONCLUSIONS

The complexity of the Bouguer anomaly in the CU of the Araguainha impact structure denotes the non-uniformity of the granites' positioning in its center. This is consistent with several previous studies indicating that the impact changed the rocks' petrophysical properties, which explains the gravity variations throughout the structure. Consequently, the density distribution model based on gravity inversion is quite irregular, and its interpretation is not straightforward. Several geological observations were considered as additional constraints and used in our model. Despite its limitations, the 3D model obtained in this study by data inversion is in agreement with previous studies. The highly variable Bouguer anomaly values at the center, and especially in the area of the granite, suggest that the rocks were strongly affected by shock wave -induced deformations and structural displacement that took place during the collapse of the transient crater and formation of the (CU). Consequently, molten and brecciated rocks were mixed into the granite, which was confirmed by the high-temperature and high-pressure peaks in the first 2 km of the granite' depth, where breccias/melts are found. Both, the gravity data and the numerical model of the structure's formation, show that the granite dips from the center outward, extending beneath the rocks of the Furnas Formation, as expected for a complex crater.

The width of 16 km, provided by the 3D Bouguer data combined with the numerical model, is a new finding for the Araguainha impact structure, as previous authors have reported it to be smaller than the one indicated in our model.

Our model reproduces the morphometry of the Araguainha structure relatively well, provided that the material strength of the sedimentary and crystalline rocks greatly varied at the time of the impact or during the crater's formation. This may imply that the sedimentary strata were mobilized by the high-water content that might have supplied by the shallow sea depositional environment, or that the strata had great anisotropic strength, with bedding planes acting as effective slip surfaces.

Acknowledgments

This study was partly financed by the Coordenação de Aperfeiçoamento de Pessoal de Nível Superior – Brazil (CAPES) – Finance Code 001. The field campaigns and the processing and modeling of the gravity data were supported by the Fundação de Amparo à Pesquisa do Estado de São Paulo (FAPESP), grant #2016/16021-5. M. Miyazaki thanks Conselho Nacional de Desenvolvimento Científico e Tecnológico (CNPq, process #132153/2016-5) for her Master's fellowship, and Marcos Vasconcelos thanks FAPESP for his postdoctoral fellowship in Brazil (#2012/04191-2) and in Germany (#2012/19726-9). Alvaro P. Crósta acknowledges a research grant from CNPq (#302679/2018-9). The authors also thank the Geophysics Laboratory of the Institute of Geosciences/Unicamp for providing the gravity meter and the GPS used in the field survey.

REFERENCES

AMSDEN AA, RUPPEL HM & HIRT CW. 1980. SALE: Simplified ALE computer program for fluid flow at all speeds. Los Alamos National Laboratory: New Mexico, 101 p. doi: 10.2172/5176006.

ANDREOLI MAG, HART RJ, COOPER GRJ, STENGEL I, WEBB S, HADDON I, SKÁLA R & VIOLA G. 2007. The 144M.a. Morokwng

impact crater, South Africa: geophysical and borehole evidence for a ~240 km structure. 10th SAGA Bienniak Technical Meeting and Exhibition, 4 p.

BANNATYNE BB & MCCABE HR. 1984. Manitoba crater revealed. GEOS 13: 10-13.

BRIGGS IC. 1974. Machine contouring using minimum curvature. Geophysics 39(1): 39-48. doi: 10.1190/1.1440410.

BRITO NEVES BB, FUCK RA & PIMENTEL MM. 2014. The Brasiliano collage in South America: a review. Braz J Geo 44(3): 493-518. doi: 10.5327/Z2317-4889201400030010.

CARPOZEN L, GILDER SA & HART RJ. 2005. Paelomagnetism of the Vredefort meteorite crater and implications for craters on Mars. Nature 435(7039): 198-201.

CHAPMAN CR & MCKINNON WB. 1986. Cratering of planetary satellites, in: BURNS JA & MATTHEWS MS (Eds). Satellites: University of Arizona Press. Tucson, p. 492-580.

COLLINS GS. 2014. Numerical simulations of impact crater formation with dilatancy. J Geophys Res Plan 119: 2600-2619.

COLLINS GS, MELOSH HJ & IVANOV BA. 2004. Modeling damage and deformation in impact simulations. Meteor & Plan Sci 39: 217-231. doi: 10.1111/j.1945-5100.2004.tb00337.x.

COLLINS GS, WÜENNEMANN K, ARTEMIEVA N & PIERAZZO E. 2012. Numerical modelling of impact processes, In: OSINSKI GR * PIERAZZO E. Impact cratering: Processes and products. Wiley-Blackwell Chichester, UK, p. 254-270. doi: 10.1002/9781118447307.ch17.

CORDANI UG, NEVES BBB, FUCK RA, PORTO R, THOMAZ FILHO A & CUNHA FMB. 1984. Estudo preliminar de integração do pré-cambriano com eventos tectônicos das bacias sedimentares brasileiras. Ciên Téc Petro. Seção: exploração de petróleo 14: 1-70.

CRÓSTA AP. 1982. Mapeamento geológico do Domo de Araguainha utilizando técnicas de sensoriamento remoto. Instituto Nacional de Pesquisas Espaciais (INPE), São José dos Campos, 90 p.

CRÓSTA AP. 1999. Araguainha Dome - The largest astrobleme in South America, in: SCHOBBENHAUS C, CAMPOS DA, QUEIROZ ET, WINGE M & BERBERT-BORN M (Eds). Sítios geológicos e paleontológicos do Brasil: http://www.unb.br/ig/sigep/sitio001/sitio001english.htm [accessed April 2016].

CRÓSTA AP, GASPAR JC & CANDIA MAF. 1981. Feições de metamorfismo de impacto no Domo de Araguainha. Rev Bras Geo 11: 139-146.

CRÓSTA AP, REIMOLD WU, VASCONCELOS MAR, HAUSER N, OLIVEIRA GJG, MAZIVIERO MV & GÓES AM. 2019. Impact cratering: The South American record – Part 1. Chemie der Erde 79: 1-61. doi: 10.1016/j.chemer.2018.06.001.

EITEL M, GILDER SA, KUNZMANN T & POHL J. 2014. Rochechouart impact crater melt breccias record no geomagnetic field reversal. Earth Plan Sci Let 387: 97-106.

ELBESHAUSEN D, WÜNNEMANN K & COLLINS GS. 2009. Scaling of oblique impacts in frictional targets: Implications for crater size and formation mechanisms. Icarus 204: 716-731. doi: 10.1016/j.icarus.2009.07.018.

ENGELHARDT WV, MATTHÄI SK & WALZEBUCK J. 1992. Araguainha impact crater, Brazil. I. The interior part of the uplift. Meteoritics 27: 442-457. doi: 10.1111/j.1945-5100.1992.tb00226.x.

ERICKSON TM, TIMMS NE, KIRKLAND EL, TOHVER E, CAVOSIE AJ, PEARCE MA & REDDY SM. 2017. Shocked monazite chronometry: integrating microstructural and in situ isotopic age data for determining precise impact ages. Cont to Min and Petro 172: 11 p. doi: 10.1007/s00410-017-1328-2.

ERNSTSON K. 1984. A gravity-derived model for the Steinheim impact crater. Geo Runds 73: 483-498. doi: 10.1007/bf01824969.

ERNSTSON K, LAMBERT P & POHL J. 1978. Gravity measurements in the Rochechouart impact structure (France). Meteoritics 13: 601-603.

FRENCH BM. 1998. Traces of Catastrophe: A Handbook of Shock-Metamorphic Effects in Terrestrial Meteorite Impact Structures. LPI Contribution 954, Lunar and Planetary Institute. Houston, 120 p.

GEOSOFT. 2016. VOXI Earth Modelling [online]. Available from http://www.geosoft.com/products/voxi-earth-modelling/ [accessed December 2016].

GIACOMINI BB, LEITE EP & CRÓSTA AP. 2017. 3D gravimetric investigation of the Cerro do Jarau structure, Rio Grande do Sul, Brazil. Meteo Plan Sci 52(4): 565-583.

GODOY AM, PINHO FEC, MANZANO JC, ARAÚJO LMB, DE SILVA JÁ & FIGUEIREDO M. 2010. Estudos isotópicos das rochas granitoides Neoproterozóicas da Faixa de Dobramento Paraguai. Rev Bras Geo 40(3): 380-391.

GRIEVE RAF, DENCE MR & ROBERTSON PB. 1977. Cratering processes: As interpreted from the occurrence of impact melts. Imp Exp Crat, Pergamin Press. New York, p. 791-814.

GRIEVE RAF, DOREEN EA, JOANNA VM & ARTEMIEVA N. 2010. The Evolution of the Onaping Formation at the Sudbury Impact Structure. Met Plan Sci 45(5): 759-782. doi:10.1111/j.1945-5100.2010.01057.x.

GRIEVE RAF & PILKINGTON M. 1996. The signature of terrestrial impact. AGSO J Au Geo Geoph 16(4): 399-420.

HAUSER N, MASSIMO M, BROWN M, NOVAIS E, CUADROS F, PEREIRA L & MAZIVIEIRO MV. 2014. Shocked Zircons from Araguainha impact structure, Brazil: textural evidences from high pressure (> 40 GPa) conditions? [abs.]

Proceedings 77th Annual Meeting of the Meteoritical Society. Casablanca. doi: 10.1111/maps.12359.

HAUSER N, REIMOLD WU, CAVOSIE AJ, CRÓSTA AP, SCHWARZ WH, TRIELOFF M, SOUZA CSM, PEREIRA LA, RODRIGUES EM & BROWN M. 2019. Linking shock textures revealed by BSE, CL, and EBSD with U-Pb data (LA-ICP-MS and SIMS) from zircon from the Araguainha impact structure, Brazil. Met Plan Sci 54(10): 2286-2311.

HENKEL H, REIMOLD WU & KOEBERL C. 2002. Magnetic and gravity model of the Morokweng impact structure. J App Geoph 49: 129-147.

HIPPERTT JP, LANA C, WEINBERG RF, TOHVER E, SCHMIEDER M, SCHOLZ R, GONÇALVES L & HIPPERTT JF. 2014. Liquefaction of sedimentary rocks during impact crater development. Earth Plan Sci Let 408: 285-295.

IVANOV BA. 2001. Mars/Moon cratering rate ratio estimates. Spa Sci Rev 96: 87-104.

IVANOV BA, DENIEM D & NEUKUM G. 1997. Implementation of dynamic strength models into 2D hydrocodes: Application for atmospheric breakup and impact cratering. Inter J Imp Eng 17: 375-386.

IVANOV BA & STÖFFLER D. 2005. The Steinheim impact crater, Germany: Modeling of a complex crater with central uplift [abs.] in 36th Annual Lunar and Planetary Science Conference 36: 1443.

JACOBY W & SMILDE PL. 2009. Gravity interpretation: fundamentals and application of gravity inversion and geological interpretation. Springer Science & Business Media, 394 p.

KOCH SA, GILDER SA, POHL J & TREPMANN C. 2012. Geomagnetic field intensity recorded after impact in Ries meteorite crater. Geoph J Inter 189(1): 383-390.

LACERDA FILHO JW, ABREU FILHO W, VALENTE CR, OLIVEIRA CC & ALBUQUERQUE MC. 2004. Geologia e Recursos Minerais do Estado de Mato Grosso. Programa Integração, Atualização e Difusão de Dados de Geologia do Brasil. CPRM/SICME-MT, MME, 235 p.

LANA C, ROMANO R, REIMOLD WU & HIPPERTT J. 2006a. Collapse of large complex impact structures: Implications from the Araguainha impact structure. Geo 34: 9-12.

LANA C, SOUZA FILHO CR, MARANGONI YR, YOKOYAMA E, TRINDADE RIF, TOHVER E & REIMOLD WU. 2007. Insights into the morphology, geometry, and post-impact erosion of the Araguainha peak-ring structure, central Brazil. Geo Soc Am Bul 119: 1135-1150. doi: 10.1130/b26142.1.

LANA C, SOUZA FILHO CR, MARANGONI YR, YOKOYAMA E, TRINDADE RIF, TOHVER E & REIMOLD WU. 2008. Structural evolution of the 40 km wide Araguainha impact structure, central Brazil. Met Plan Sci 43: 701-716. doi: 10.1111/j.1945-5100.2008.tb00679.x.

LI X & GÖTZE H. 2001. Ellipsoid, geoid, gravity, geodesy, and geophysics. Geophysics 66: 1660-1668.

LI Y & OLDENBURG DW. 1998. 3-D inversion of gravity data. Geophysics 63: 109-119. doi: 10.1190/1.1444302.

MACHADO R, LANA C, SOUZA FILHO CR & STEVENS G. 2008. Optical and scanning electron microprobe study of shock veins from the Araguainha central uplift, central Brazil [abs.] in IV Large Meteorite Impacts and Planetary Evolution Conference. Vredefort Dome, South Africa: 3062.

MARANGONI YR, SANTON DS, VASCONCELOS MAR, MOLINA EC, VIEIRA CD, LANA C, DE SÁ NC, SOUZA FILHO CR & TRINDADE R. 2007. Gravity at Araguainha Impact Structure: Preliminary Results [abs] in 10th International Congress of the Brazilian Geophysical Society. Rio de Janeiro, Brazil: 1852-1857. doi: 10.1190/sbgf2007-360.

MARANHÃO MSAS & PETRI S. 1996. Novas ocorrências de fósseis nas formações Corumbataí e Estrada Nova do estado de São Paulo e considerações preliminares sobre seus significados paleontológico e bioestratigráfico. Rev Inst Geo 17: 33-54. doi: 10.5935/0100-929x.19960002.

MASERO W, FISCHER G & SCHNEGG PA. 1997. Electrical conductivity and crustal deformation from magnetotelluric results in the region of the Araguainha impact, Brazil. Phys Earth Plan Int 101: 271-289. doi: 10.1016/s0031-9201(96)03267-0.

MASERO W, SCHNEGG PA & FONTES SL. 1994. A magnetotelluric investigation of the Araguainha impact structure in Mato Grosso-Goiás, central Brazil. Geoph J Inter 116: 366-376. doi: 10.1111/j.1365-246x.1994.tb01803.x.

MELOSH HJ. 1979. Acoustic fluidization: A new geologic process? J Geoph Res 84: 7513-7520. doi: 10.1029/jb084ib13p07513.

MELOSH HJ. 1989. Impact Cratering: A Geologic Process. Oxford University Press. New York, 245 p.

MELOSH HJ. 2007. A hydrocode equation of state for SiO2. Met Plan Sci 42: 2079-2098. doi: 10.1111/j.1945-5100.2007.tb01009.x.

MELOSH HJ & IVANOV BA. 1999. Impact crater collapse. An Rev Earth Plan Sci 27: 385-415. doi: 10.1146/annurev.earth.27.1.385.

MELOSH HJ, RYAN EV & ASPHAUG E. 1992. Dynamic fragmentation in impacts: Hydrocode simulation of laboratory impacts. J Geoph Res 97: 14735-14759.

MILANI EJ, MELO JHG, SOUZA PA, FERNANDES LA & FRANÇA AB. 2007. Bacia do Paraná. Bol de Geo Petro 15: 265-287.

PEREIRA E, CARNEIRO CDR, BERGAMASCHI S & ALMEIDA FFM. 2012. Evolução das sinéclises paleozóicas: Províncias Solimões, Amazonas, Parnaíba e Paraná, in HASUI Y, CARNEIRO CDR, ALMEIDA FFM & BARTORELLI A (Eds) Geologia do Brasil. São Paulo, p. 374-394.

PIERAZZO E, VICKERY AM & MELOSH HJ. 1997. A reevaluation of impact melt production. Icarus 127: 408-423. doi: 10.1006/icar.1997.5713.

PILKINGTON M & GRIEVE RAF. 1992. The geophysical signature of terrestrial impact craters. Rev Geo 30: 161-181. doi: 10.1029/92rg00192.

REIMOLD WU, HAUSER N & CRÓSTA AP. 2018. The impact recordo f SW Gondwana, in: SIEGESMUND S, BASEI MAS, OYHANTÇABAL P & ORIOLO S (Eds) Geology of Southwest Gondwana, Regional Geology Reviews. Spinger, p. 677-688.

SCHNEGG PA & FONTES SL. 2002. Feasibility study of the geoelectric structure of the Araguainha impact, Brazil. Earth, Plan Spa 54: 597-606. doi: 10.1186/bf03353048.

SILVA D, LANA C & SOUZA FILHO CR. 2016. Petrographic and geochemical characterization of the granitic rocks of the Araguainha impact crater, Brazil. Met Plan Sci 51: 1-25. doi: 10.1111/maps.12601.

THOMPSON SL & LAUSON HS. 1972. Report SC-RR- 710714: Sandia Labs Albuquerque, New Mexico, 119 p.

TOHVER E, LANA C, CAWOOD PA, FLETCHER IR, JOURDAN F, SHERLOCK S, RASMUSSEN B, TRINDADE RIF, YOKOYAMA E, SOUZA FILHO CR & MARANGONI Y. 2012. Geochronological constraints on the age of a Permo-Triassic impact event: U-Pb and $^{40}Ar/^{39}Ar$ results for the 40 km Araguainha structure of central Brazil. Geochim Cosmochim Acta 86: 214-227. doi: 10.1016/j.gca.2012.03.005

TONG CH, LANA C, MARANGONI YR & ELIS VR. 2010. Geoelectric evidence for centripetal resurge of impact melt and breccias over central uplift of Araguainha impact structure. Geology 38(1): 91-94.

VASCONCELOS MAR. 2007. Caracterização geofísica da estrutura de impacto de Araguainha (MT/GO). MS thesis, IAG-USP. São Paulo, 175 p.

WÜNNEMANN K, COLLINS GS & MELOSH HJ. 2006. A strain-based porosity model for use in hydrocode simulations of impacts and implications for transient crater growth in porous targets. Icarus 80: 514-527. doi: 10.1016/j.icarus.2005.10.013.

WÜNNEMANN K & IVANOV BA. 2003. Numerical modelling of crater depth-diameter dependence in acoustically fluidized target. Planet Space Sci 51: 831-845. doi: 10.1016/j.pss.2003.08.001.

YOKOYAMA E, TRINDADE RIF, LANA C, SOUZA FILHO CR, BARATOUX D, MARANGONI YR & TOHVER E. 2012. Magnetic fabric of Araguainha complex impact structure (Central Brazil): implications for deformation mechanisms and central uplift formation. Earth Planet Sci Lett 331: 347-359.

ZIVKOVIC VB. 2012. A geophysical investigation of the northeastern rim of the St. Martin impact structure, Manitoba, Canada [Ph.D] University of North Dakota, 61 p.

How to cite

MIYAZAKI MR, LEITE EP, VASCONCELOS MAR, WÜNNEMANN K & CRÓSTA AP. 2021. Bouguer anomaly inversion and hydrocode modeling of the central uplift of the Araguainha impact structure. An Acad Bras Cienc 93: e20210081. DOI 10.1590/0001-3765202120210081.

Manuscript received on January 20, 2021;
accepted for publication on July 21, 2021

MARCELLE R. MIYAZAKI[1]
https://orcid.org/0000-0002-4528-7565

EMILSON P. LEITE[1]
https://orcid.org/0000-0003-1691-6243

MARCOS A.R. VASCONCELOS[2]
https://orcid.org/0000-0002-4970-0484

KAI WÜNNEMANN[3,4]
https://orcid.org/0000-0001-5423-1566

ALVARO P. CRÓSTA[1]
https://orcid.org/0000-0003-0485-1147

[1]Instituto de Geociências, Universidade Estadual de Campinas, Rua Carlos Gomes, 250, 13083-855 Campinas, SP, Brazil

[2]Universidade Federal da Bahia, Instituto de Geociências, Departamento de Geofísica, Av. Adhemar de Barros, s/n, 40170-110 Salvador, BA, Brazil

[3]Museum für Naturkunde, Leibniz Institute for Evolution and Biodiversity Science, Invalidenstraße 43, 10115 Berlin, Germany

[4]Freie Universität Berlin, Malteserstr., 74-100, Haus D, 12249 Berlin, Germany

Correspondence to: **Emilson Pereira Leite**
E-mail: emilson@unicamp.br

Author contributions

Marcelle Rose Myazaki: Data acquisition; Data processing and analysis; Gravity inversions; Geological interpretations; Writing. Emilson Pereira Leite: Data acquisition; Computer programming; Data analysis; Gravity inversions; Writing. Marcos Alberto Rodrigues Vasconcelos: Data collection; Numerical modelling; Geological interpretations; Writing. Kai Wünnemann: Numerical modelling; Writing. Alvaro Penteado Crósta: Geological interpretations; Writing.